Visual Analysis of Aneurysm Data using Statistical Graphics

Monique Meuschke, Tobias Günther, Philipp Berg, Ralph Wickenhöfer, Bernhard Preim, Kai Lawonn

Abstract—This paper presents a framework to explore multi-field data of aneurysms occurring at intracranial and cardiac arteries by using statistical graphics. The rupture of an aneurysm is often a fatal scenario, whereas during treatment serious complications for the patient can occur. Whether an aneurysm ruptures or whether a treatment is successful depends on the interaction of different morphological such as wall deformation and thickness, and hemodynamic attributes like wall shear stress and pressure. Therefore, medical researchers are very interested in better understanding these relationships. However, the required analysis is a time-consuming process, where suspicious wall regions are difficult to detect due to the time-dependent behavior of the data. Our proposed visualization framework enables medical researchers to efficiently assess aneurysm risk and treatment options. This comprises a powerful set of views including 2D and 3D depictions of the aneurysm morphology as well as statistical plots of different scalar fields. Brushing and linking aids the user to identify interesting wall regions and to understand the influence of different attributes on the aneurysm's state. Moreover, a visual comparison of pre- and post-treatment as well as different treatment options is provided. Our analysis techniques are designed in collaboration with domain experts, e.g., physicians, and we provide details about the evaluation.

Index Terms—Medical visualizations, aneurysms, blood flow, parametrization

✦

1 INTRODUCTION

Aneurysms are dilatations of arteries, where their evolution and progression are not well understood [8]. Their rupture leads to a bleeding, which often ends in death. Frequently, aneurysms are discovered by chance and do not lead to complications. [52]. Cerebral aneurysms with a diameter of more than 7 *mm* and aortic aneurysms with a diameter of more than 4.5 *cm* are usually treated. However, even small, inconspicuous aneurysms can rupture. A common treatment is stenting, where a metal implant (stent) is inserted into the supporting vessel of the aneurysm. However, especially cerebral aneurysms are difficult to treat, due to the long and complex way the doctor has to navigate the stent into the parent vessel. Treatment can increase the rupture risk, which can exceed the original risk [9]. Thus, a better understanding of the individual rupture risk is needed to only treat high-risk patients.

Medical studies implied several morphological features such as aneurysm location, size, and shape as risk factors for rupture [6, 28]. However, these attributes allow no reliable estimation of the individual risk. Quantitative hemodynamic attributes such as wall shear stress (WSS) or pressure as well as qualitative features, e.g., vortices seem to influence the aneurysm state [8,9]. The WSS probably triggers vascular remodeling leading either to stronger or weaker wall conditions, where rupture occurs if WSS exceeds the wall strength.

Four-dimensional phase-contrast magnetic resonance imaging (4D PC-MRI) [15] measures flow data non-invasively, usable for larger arteries, e.g., the aorta. In contrast, Computational Fluid Dynamic (CFD) approaches and Fluid-Structure Interaction (FSI) simulate flow and wall mechanics in smaller cerebral arteries [22]. Both methods result in time-dependent flow data, representing one cardiac cycle. Medical researchers compare these data between ruptured and non-ruptured cases as well as between different stent options to assess the rupture risk and to find an optimal treatment. Of particular interest is whether there are *correlations between flow and wall-related attributes*

- *Monique Meuschke is with University of Magdeburg, Germany, and Research Campus STIMULATE. E-mail: meuschke@isg.cs.uni-magdeburg.de.*
- *Tobias Günther is with the ETH Zürich, Switzerland. E-mail: tobias.guenther@inf.ethz.ch.*
- *Philipp Berg is with University of Magdeburg, Germany, and Research Campus STIMULATE. E-mail: philipp.berg@ovgu.de.*
- *Ralph Wickenhöfer is with the Heart of Jesus Hospital in Dernbach, Germany. E-mail: r.wickenhoefer@krankenhaus-dernbach.de.*
- *Bernhard Preim is with University of Magdeburg, Germany, and Research Campus STIMULATE. E-mail: bernhard@isg.cs.uni-magdeburg.de.*
- *Kai Lawonn is with the University of Koblenz-Landau, Germany. E-mail: lawonn@uni-koblenz.de.*

such as wall thickness leading to an increased rupture risk. Here, also the homogeneity of attributes is investigated. Experts assume that the thinner the wall and the more inhomogeneous attributes such as WSS or pressure are, the higher the risk of rupture. However, the analysis of the complex data is time-consuming and challenging.

We developed a visualization framework in close cooperation with medical doctors to improve the aneurysm rupture risk and treatment assessment. Our tool enables a comparison of ruptured and non-ruptured cases as well as pre- and post treated data with different stent configurations. Several views allow an efficient analysis of attribute correlations over the cardiac cycle. This includes a novel 2D plot-based visualization providing a temporal overview about correlations between scalar attributes. For a more detailed analysis, we provide a 2D map-based and a 3D depiction of the aneurysm morphology linked to statistical plots, comprising scatterplots and histograms of scalar attributes. Brushing and linking techniques aid the user to study risky correlations. We provide 2D aneurysm maps for both types of aneurysm shapes, saccular and fusiform aneurysms, see Fig. 1, which was not possible so far. Moreover, a novel glyph design allows a simultaneous exploration of two scalar fields at risky wall regions. This is further supported by a time-dependent clustering of attributes to identify heterogeneous and homogeneous regions. In summary, our main contributions are:

- A combination of 2D and 3D visualizations as well as statistical plots to analyze attributes on the aneurysm wall simultaneously.

- A novel approach to generate 2D maps of fusiform aneurysms.

- Novel concepts such as a 2D plot-based depiction and glyphs to analyze time-dependent attribute correlations more quantitatively.

2 RELATED WORK

Related work comprises multi-attribute exploration using information visualization, time-dependent data visualization using glyphs, and the visual exploration of aneurysm data.

2.1 Information Visualization to explore Simulated Data

Our work is related to previous attempts to the feature-based analysis of flow simulation results with information visualization techniques. An early example is the WEAVE system [19], where cardiac simulation data is mapped to the heart anatomy and to scatterplots and histograms that are integrated in multiple coordinated views. Thus, brushing allows to specify features in the attribute space and linking highlights corresponding locations on the heart surface. A prominent example for this line of research is the SimVis system [13, 14] that provides advanced scatterplots, scatterplot matrices and parallel coordinate views

to extract features of simulations, primarily in the context of time-dependent simulation of vehicle dynamics. Feature-based analysis in time-dependent data involves *feature tracking* over time [23].

2.2 Visualization of Multi-Field Data using Glyphs

Simulation results comprise multiple fields of values that can effectively be visualized by using glyphs. Borgo et al. [7] presented general guidelines for glyph design. Ropinski et al. [43] introduced a taxonomy for glyph-based medical visualizations, focused on diffusion tensors and cardiac data. Superquadrics are commonly used to visualize diffusion tensors by mapping the eigenvalues and eigenvectors of the tensor to its shape and orientation [25]. Related to this, Meuschke et al. [36] compared several 2D and 3D glyphs to visualize tensor data of aneurysms describing mechanical wall shear forces. Rocha et al. [42] applied sets of images, called *decal-maps* to the aneurysm surface representing different attributes. However, these glyphs are not appropriate to show the temporal behavior of scalar data. Therefore, van Pelt et al. [51] used tailor-made glyphs to show the influence of various stent scenarios on scalar attributes over time. The main drawbacks are the limited number of depicted time steps and the lack of presenting quantitative information. Similar to our work, Tominski et al. [48] visualized spatio-temporal data on maps by using the different sides of pencil and helix icons. Meuschke et al. [35] used bar charts applied to aneurysm data to show two attributes over time using the bars' height and bars' color.

2.3 Visual Exploration of Aneurysm Data

Next, we describe approaches to visualize the aneurysm morphology. Techniques to analyze qualitative flow features are neglected, since our work focuses the depiction of scalar data mapped on the aneurysm wall.

To facilitate data analysis, abstract surface depictions are generated by using parametrization approaches. For a combined exploration of the morphology and scalar data, Neugebauer et al. [40] used several 2D projections from different perspectives. In [18], the aneurysm is represented by a uniform sphere to analyze WSS. Meuschke et al. [35] used *least squares conformal maps* [31] to generate a 2D aneurysm map that serves as an overview visualization. The *VesselMap* [47] is a 2D map of an aneurysm and adjacent vasculature generated by an graph-based optimization. Inspired by the cardiac *Bull's Eye Plot (BEP)*, an occlusion-free 2D plot to explore one scalar field of aortic flow data was presented by Köhler et al. [26]. The angular and radial segments of the plot represent the time steps and aortic segments, respectively. Meuschke et al. [34] extended this plot by discretizing the radius into four segments based on four anatomical sections of the aorta.

Other works support the visual exploration of morphological features based on 3D vessel surfaces. Inspired by the suggestive contour measure, Lawonn et al. [30] presented an illustrative surface visualization. Based on the local curvature of the surface, the transparency is adapted, which emphasizes convex and concave regions. Van Pelt et al. [50] combined cel shading and vessel silhouettes to generate an abstract vessel depiction. However, scalar attributes are not visualized. The tool by Glaßer et al. [17] provides a hierarchical clustering of WSS and wall thickness for a single time step to find suspicious wall regions. However, a simultaneous depiction of two arbitrary scalar fields is not allowed. To detect spots of fluid wall interaction, Meuschke et al. [35] presented a simultaneous exploration of two attributes on the aneurysm wall by using color-coding and image-based hatching. However, the discretization of attribute ranges into four hatching textures reduces the quantitative analysis of the illustrated data.

Contribution Summary. To explore multi-field aneurysm data, we combine information and scientific visualizations by using multiple coordinated views. We use a GPU-based implementation of statistical plots to show the temporal behavior of scalar data with interactive frame rates. We integrate a 2D aneurysm map to further support data exploration. Existing maps [18, 35, 40] are restricted to saccular aneurysms, where one surface, called *ostium*, separates the aneurysm from the parent vessel. Aortic aneurysms, however, are often elongated dilatations in which there are two

ostium areas existing. We introduce a novel mapping to handle their cylindrical shape. In addition, we present novel techniques that support a simultaneous exploration of multiple attributes.

Fig. 1. Aneurysm shapes.

We propose a 2D plot that provides an overview of multiple attributes over time instead of depicting just a single quantity [26, 34]. For a more detailed analysis of attribute correlations on a specific surface region, we introduce a checkerboard visualization and provide novel glyphs to show the temporal behavior of scalar data. The checkerboard approach overcomes the reduced ability of a quantitative analysis using image-based hatching [35]. Compared to the glyph design by Tominski et al. [48], we combine cylindrical glyphs with disk-shaped glyphs that do not require manual rotations to explore attributes. Moreover, we extend the clustering by Glaßer et al. [17] to multiple time-dependent attributes, which allows a more detailed risk assessment.
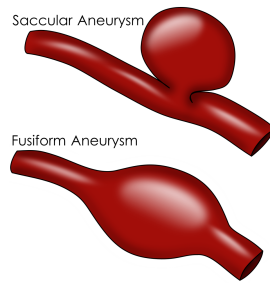
3 DATA ACQUISITION AND PREPROCESSING

This section describes the acquisition and preprocessing of aneurysm data, see Fig. 2. This comprises the vessel surface extraction, the calculation of flow data and the virtual stenting for simulated data.

3.1 Measured Flow Data

The 4D PC-MRI data are acquired by a 3 T Siemens Magnetom Verio MR scanner with a maximum expected velocity of 1.5 *m/s* per dimension. For each direction (x, y and z), time-resolved flow and magnitude images are determined describing direction and strength of the flow, respectively. For the spatial domain 15 to 23 slices are acquired with a grid size of 132×192 voxels covering $1.77 \times 1.77 \times 3.5$ mm^3. Between two of the 14 to 21 time steps, a distance of $50\,ms$ exists. Artifacts in the flow images, considering Phase wraps [12] and velocity offsets [29] are corrected using the magnitude images. Then, a temporal maximum intensity projection [50] is calculated as basis for a binary segmentation. For each voxel the flow velocity is considered and the maximum is taken from all time steps. This leads to a good contrast everywhere where fast flow over time occurs. This reduces the 4D image to a high-contrast 3D image. From this 3D image, the vessel surface is extracted via Marching Cubes.

3.2 Simulated Flow Data

First, the vessel surface is extracted from contrast-enhanced CT data using the pipeline by Mönch et al [37]. Segmentation errors are manually corrected and the mesh quality is optimized [44]. For the simulation, an unstructured volumetric grid is generated from the surface.

Virtual Stenting. To simulate different treatment scenarios, a fast virtual stent deployment approach is chosen [3]. This explicit methodology allows for the consideration of each individual stent strut. This method can be applied within seconds without being computationally expensive, because it uses a geometric deformation.

CFD Simulation. The volume meshes have a size of 1.11-2.01 million cells and 5.2-8.3 million cells for the pre- and post-stenting cases, respectively. Flow measurements of a healthy volunteer are used as inlet boundary conditions [5] due to the absence of patient-specific data. A rigid wall is assumed for the vessel and the stent and the outlet pressure is set to zero. Solving Navier-Stokes equations lead to patient-specific flow information, where blood is considered as an incompressible Newtonian fluid. [4]. Three cardiac cycles with a time step size of $\Delta t = 0.001s$ are calculated. To avoid inaccuracies from initialization, only the last cycle was used for analysis.

Fluid-Structure Simulation. For some non-stented datasets, we performed FSI simulations. Inside the fluid domain, CFD is used to solve hemodynamics. The wall domain is discretized and local strains and stresses are calculated. At the transition of both domains, physical quantities such as shear forces, pressure, deformation and velocity are
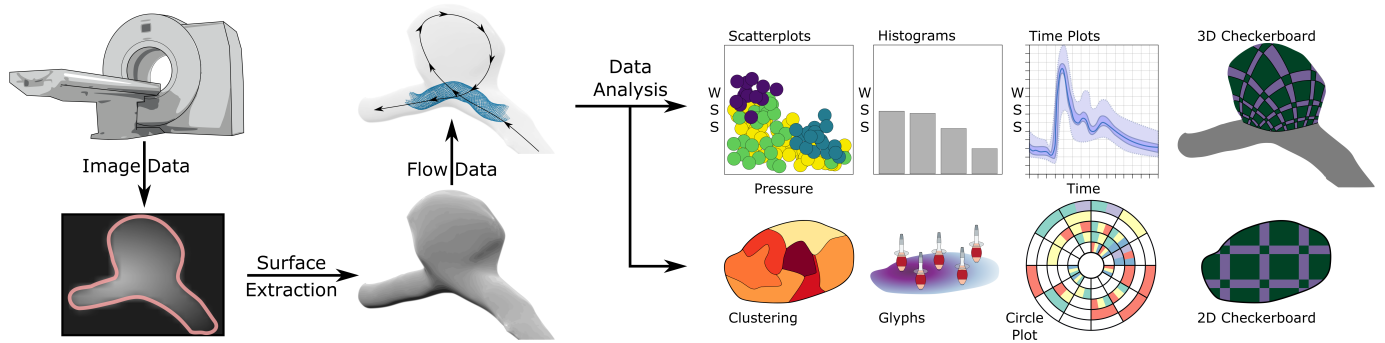
Fig. 2. Pipeline of our approach to visualize aneurysm data. First, the surface is reconstructed from clinical images as input for the virtual stenting and CFD simulation. To explore the flow data, we combine information and scientific visualizations.

exchanged over time. A deformable, homogeneous, isotropic and linear elastic wall is assumed. Due to the limited resolution of radiologic images, the wall thickness is set in the range of 0.2 to 0.6 *mm* [49] obtained from normal wall extrusion. To avoid rigid body motion, the cross-sectional planes of vessel in- and outlets are fixed.

3.3 Datasets

In this work 16 datasets are considered, see Tab. 1. We use measured flow data of two fusiform aortic aneurysms and 14 simulated cerebral cases, where one aneurysm has a fusiform shape and 13 aneurysms have a saccular shape. Four saccular aneurysms are virtually stented, where one aneurysm was ruptured in reality. For the remaining cases, just pre-treated data exists, where four saccular aneurysms are ruptured.

Table 1. Summarizing information about our used datasets.

Case (C)	Location	Shape	Ruptured	Virtually Stented	Flow Data
C 1-2	aortic	fusiform	unruptured	non-stented	measured
C 3	cerebral	fusiform	unruptured	non-stented	simulated
C 4-8	cerebral	saccular	unruptured	non-stented	simulated
C 9-12	cerebral	saccular	ruptured	non-stented	simulated
C 13-15	cerebral	saccular	unruptured	stented	simulated
C 16	cerebral	saccular	ruptured	stented	simulated

4 REQUIREMENT ANALYSIS

In clinical routine, aneurysm treatment is based on medical guidelines that consider only morphological features [46]. For a more reliable risk assessment, medical and CFD researchers try to identify risky fluid-wall interactions. Our tool should support researchers in this process. For this purpose, several requirements are defined in collaboration with three domain experts comprising two neuroradiologists with 14 and 16 years of experience and one CFD engineer with seven years of experience. Important tasks of research physicians are to estimate rupture risk and to find an optimal treatment. In contrast, CFD researchers must validate the simulation results in terms of physical plausibility.

We discussed the research workflow to analyze aneurysm data with the experts. Occurring difficulties are used to derive requirements. Since, it is still unclear, which attributes and correlations between them promote rupture, the physicians investigate color-coded attributes, e.g. WSS and pressure, on the aneurysm surface. Of particular interest are additional bulges on the aneurysm, called blebs. Such structures indicate remodeling due to inflammatory processes within the vessel wall probably leading to a lower stability. The CFD experts proceed similarly to detect incorrect simulation assumptions. In addition, the homogeneity of attributes within regions is explored, since strongly varying quantities may indicate endangered regions. To analyze the data over time, animations are utilized, whereby only one attribute is encoded at a time. Exploring a single time step is not sufficient because it is not known at which point in the cardiac cycle the rupture risk is maximum. However, animation-based exploration needs a lot of user interaction to detect hotspots of fluid-wall interaction. Moreover, different attributes have to be explored one after the other, which is

mentally exhausting. This can only be slightly improved by side-by-side views, since they only allow to analyze few time steps and attributes and it is exhaustive to mentally put these multiple images together.

The goal is to tailor a framework such that experts can efficiently analyze scalar fields and their correlations over the cardiac cycle. In addition, a simplified representation of the morphology is needed such that the aneurysm can be observed without time-consuming interactions such as rotation and zooming. Moreover, the physicians stated that an overview depiction of existing attributes and possible correlations between them would simplify the in-depth exploration of specific surface regions. Furthermore, they wished to have the possibility to explore selected surface regions. With this, vessel wall changes such as blebs could be investigated in detail to assess the rupture probability at these regions. Besides this, aneurysm stenting leads to different scalar quantities on the wall. Furthermore, different stent locations are possible, where the physician has to decide for the best choice. For this purpose, techniques are needed that visualize differences of scalar quantities before and after stenting as well as a comparison of different stent scenarios. Related to this is the visualization of differences between ruptured and non-ruptured datasets. This is important to identify rupture-prone attribute thresholds, which might lead to a more reliable risk assessment. Based on these discussions and on literature search, we summarize the main requirements as follows:

R. 1 Simultaneous analysis of different scalar fields.

R. 2 A simplified representation of the aneurysm surface.

R. 3 A visual overview showing attribute correlations over time.

R. 4 A clustering showing how homogeneous regions are.

R. 5 Visualizing the change of attributes over the cardiac cycle.

R. 6 Brushing and linking facilities to visually find coherence between different visualizations of the aneurysm.

R. 7 A comparison of ruptured and non-ruptured datasets as well as pre- and post-treated data including different stent scenarios.

5 EXPLORATION OF ANEURYSM DATA

We provide a framework that consists of four equally-sized linked views. The first view comprises a novel 2D plot that shows existent attributes and their correlations over the cardiac cycle (see Sec. 5.3, Fig. 5). In the remaining views, the aneurysm data is presented in an animated manner, representing the cardiac cycle, where the animation time is consistent between the views. The second view shows scatterplots and histograms of scalar quantities (see Sec. 5.2, Fig. 8). The third view presents a 3D aneurysm visualization, whereas a 2D aneurysm map (see Fig. 6) is displayed in the fourth view (see Sec. 5.4). On the map, glyphs can be activated showing the temporal behavior of selected scalar fields (see Sec. 5.4.2, Fig. 11). In the following, we describe the individual views and their interactive connection in more detail. We start with an explanation how the 2D aneurysm map is calculated, since some of our visualization techniques are based on this representation.

5.1 Calculation of the 2D Aneurysm Map

Aneurysms could have irregularly deformed shapes, which complicates the simultaneous exploration of attributes in 3D. Manual rotations are needed to detect critical wall regions, which is further complicated due to the time-dependent data. Similar to Meuschke et al. [35], we provide a 2D map of the aneurysm to simplify data analysis. However, their approach can only handle saccular aneurysms, which occur more frequently in cerebral arteries. In contrast, our method can also handle fusiform aneurysms, which occur more frequently in cardiac arteries. The map generation is based on the 3D aneurysm surface part, separated from the parent vessel. In the following, we describe how we determine the aneurysm part and the mapping for both aneurysm shapes.

Saccular Aneurysm Mapping. Recently, Meuschke et al. [33] proposed an automatic approach to detect the ostium of saccular aneurysms based on extracting the skeleton [2]. First, a thinning operation is applied to the surface mesh. Then edges are collapsed to obtain a skeleton, which was employed to identify the aneurysm. We use their technique to automatically determine the ostium. The aneurysm surface part is yielded by cutting the 3D surface along the detected ostium. Afterwards, the aneurysm surface is parameterized to the 2D domain. Such parameterizations can be roughly divided into angle-preserving and area-preserving maps, where there are also methods that try to combine both mappings. We need an angle-preserving map, as we want to display a checkerboard texture on the 2D map to explore two attributes simultaneously and then project this onto the 3D surface. Therefore, we apply *spectral conformal parameterization* (SCP) [39]. Unfortunately, length distortions are inevitable. To reduce the distortion, we further process the vertices on the 2D domain according to Zayer et al. [53]. The vertices are iteratively moved such that the length distortion is reduced by holding the conformal condition. The one-time necessary computation of the map takes between 1.1 and 6.8 s, depending on the number of mesh triangles.

Fusiform Aneurysm Mapping. The principle idea of the fusiform mapping is to determine cylindrical coordinates that represent the cylindrical aneurysm shape. Our parameterization was inspired by a geodesic parameterization approach [41] and the straightening approach developed by Angelelli and Hauser [1]. According to parameterization approaches in the field of colonoscopy [27], two works are related to the flattening of fusiform aneurysms [20,21]. These are the only ones that just need the mesh as input. Nevertheless, for the flattening of the surface mesh the end regions need to be cut open to generate a genus 1 mesh. In contrast, our algorithm works automatically without additional user-input. Angelelli and Hauser employed the vessel centerline and created consecutive planes along the centerline. Vertices on the vessel mesh between these planes need to be identified and the space defined by these planes is transformed such that the vertices are stacked. Contrarily, we generate the vessel skeleton with the method by Au et al. [2]. This has the advantage that every point on the skeleton corresponds to vertices on the original mesh after creating the skeleton. With this, we can easily straighten the skeleton and apply the same transformation to the corresponding vertices on the mesh, see Fig. 3. For this, we define a direction, e.g., $(1,0,0)$ as the height direction. Afterwards, we start with an endpoint of the skeleton and determine the consecutive tangent vectors along the skeleton. For every point on the skeleton, we use the previously determined tangent vector and rotate it such that it coincides with the direction vector. The same transformation is applied to the corresponding mesh vertices, which results in a straightened vessel. For every vertex on the straightened vessel, we determine the corresponding height and angle, resulting in cylindrical coordinates. Afterwards, the user needs to define the beginning and ending of the aneurysm by clicking on the surface. The part between the selected vertices is easily extracted by considering only this part, whose height is between them. Afterwards, we roll the part out, see Fig. 4. The generation of the fusiform maps takes between 4.3 and 9.6 s due to the thinning operation. Note that we encountered only datasets with fusiform aneurysms without furcations, which results in only two endpoints. In case of a dataset with a fusiform aneurysm and furcations, we could ask the user first to select the beginning and the ending of the
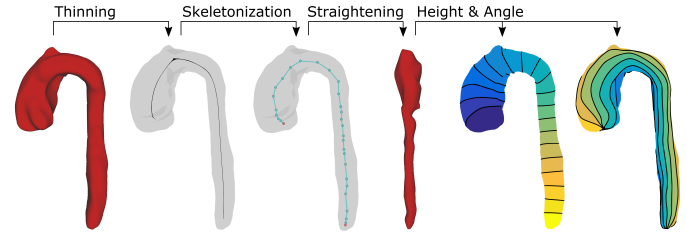

Fig. 3. Parametrization of a fusiform aortic aneurysm (C1). On the 3D mesh, a thinning operation is performed. Then, edges are collapsed resulting in the skeleton. A straightening approach leads to a cylindrical shape of the aorta, which yields the height and the angle for the parameterization.

aneurysm, which are then used to detect the correct part on the skeleton, which can then be used for the straightening.
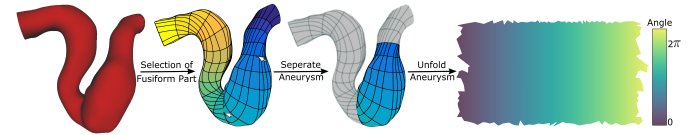

Fig. 4. Unfolding of a parametrized cerebral fusiform aneurysm (C3). The user selects two points on the surface defining the aneurysm start and end region, where the height is color-coded by a dark blue-to-yellow color map. Then, the aneurysm part is unfolded, where here the angle is color-coded.

5.2 Multi-Field Correlation Analysis using the Circle Plot

Measured and simulated flow data describe one full heart cycle, from which multiple attributes can be extracted such as WSS, pressure, wall thickness, wall deformation, or stress according to Mises (stress in the wall caused by deformation). Cerqueira et al. [10] introduced the BEP. In clinical routine, this is a commonly used 2D plot to visualize quantitative perfusion data of the left ventricle at a glance. Since clinicians are used to the representation by round plots, we developed a 2D circle plot presenting possible correlations between scalar fields over the cardiac cycle, see Fig. 5 (R. 3). The plot presents an analogy to a clock, which is reasonable to depict periodic time-dependent data. With this, interesting surface regions and time steps according to occurring scalar values can be detected without an exhausting exploration in 3D using animations.

Fig. 5. Circle plot to show occurring attribute correlations.

For this purpose, the plot area is decomposed into T equal parts, where T is the number of acquired time steps. Based on the design of a clock, the first time step starts at 12 o'clock; the direction is clockwise. Due to the large number of time steps (up to 93 in simulated data), the user can reduce the number of presented time steps. In Fig. 5, every third time step is used. This is a reasonable simplification, since the scalar changes between two time steps are quite low for such a high temporal resolution. Then, each of these sectors is subdivided into S equally large segments along the radius r, where S is the number of scalar fields in the dataset. A legend in the top left corner shows the order of the scalar fields along the radius, where each quantity is represented by the first three initial letters.

In the center of the plot, a 2D map is shown, which is subdivided into five colored regions. Each aneurysm vertex is assigned to one of these regions. Moreover, the expert can manually define a threshold for each scalar field. If there is an aneurysm vertex where the current scalar value is greater than or equal to the threshold, the corresponding
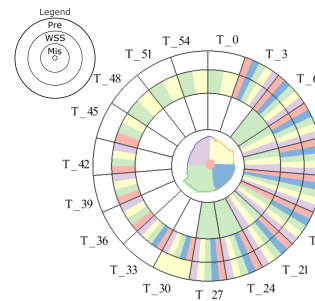
temporal plot region is colored to the vertex's region color. For example, at T_{24}, within the red region, there is a lower stress according to Mises than the defined threshold (no red area on the innermost segment), but the WSS and pressure exceed the selected thresholds. In case that more than one map region fulfills the thresholds, the corresponding plot segments are further subdivided.

Region Division. As an entry point for exploration, we define an initial region division. For saccular aneurysms, we divide the map into five regions with a similar surface area, see Fig. 6. One region should represent the aneurysm dome (red area), since this is a rupture-prone area. Around the dome, we generate four more regions. First, we need a target area for each region given by $\frac{1}{5}A_{Aneu}$, where A_{Aneu} is the total aneurysm area.

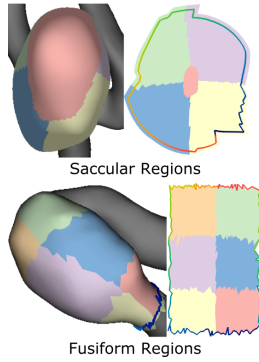Saccular Regions

Fusiform Regions

Fig. 6. Region devision for saccular and fusiform aneurysms.

Second, we extract the vertex with the largest geodesic distance from the boundary, i.e., the dome point, using the heat method [11]. From the dome point, we look for a geodesic distance such that the inscribed area approximates the target area. The geodesic distance can be determined with the golden-section search [24]. The inscribed area yields the first region R_1. Then, we use a sweep line from left to right, with respect to the coordinates of the 2D map. Again, the golden-section search yields a position such that the remaining area is divided in half. For each half, we search for the horizontal line such that both areas approximate the target area. This yields region R_2, R_3 for the left part and R_4, R_5 for the right part. For fusiform aneurysms, six regions are generated based on the rectangular shape of the 2D map, see Fig. 6. Based on the cylindrical coordinates, two regions are placed along the angle and three regions are defined along the height.

Plot Interactions. There are different options to interact with the circle plot. Initially, the thresholds for each scalar field are set to one third of the corresponding range. If a threshold is changed, the coloring of the plot segments is updated in real time. This shows immediately if there is a wall region that fulfills the selected thresholds. Moreover, the user can brush individual regions on the 2D map or the 3D surface, where a 'C' is rendered in the plot center to indicate the 'Custom' region brushing. The aneurysm in Fig. 7 exhibits multiple blebs that are brushed. Here, a low wall thickness and WSS as well as an increased pressure are selected as thresholds. Only the blueish region fulfills all conditions, which indicates a possible rupture area. To explore this region in more detail, the plot segments can be selected, where the selected segment is highlighted. Then, the animation time is set to the selected time step and a contour rendering is activated on the 2D map and the 3D surface to uncover the selected scalar field.
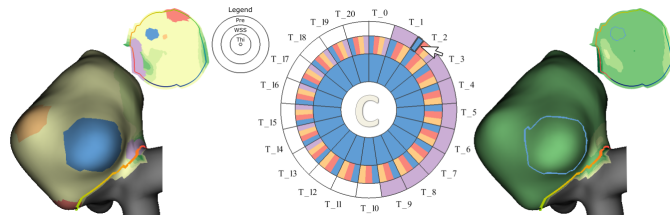

Fig. 7. Brushing of morphologically suspicious regions of C7 used to color the plot. Here, a low wall thickness and WSS as well as an increased pressure are selected as thresholds, which comply with the bluish bleb. A contour rendering is activated for a chosen plot segment.

5.3 Multi-Field Analysis using Statistical Plots

The second view shows a matrix-based visualization that enables a comparison of different datasets, see Fig. 8 (R. 7). Each entry of the matrix represents a combination of two scalar fields. Statistical plots are shown that give an overview of the distribution of scalar quantities. Thereby, the upper triangle matrix represents the first case, e.g., a non-ruptured case. In the lower triangle matrix another case can be loaded, e.g., a ruptured aneurysm. Otherwise, the corresponding matrix entries show also the first case. In the remaining views only the first case is visualized to reduce the visual complexity.

The non-diagonal entries of the matrix present scatterplots for each scalar field combination. The diagonal entries are used for a histogram that shows occurring values of the corresponding scalar field. To show the histograms for both datasets, the diagonal entries are splitted and show on top the histograms of the first case and below the values of the second case. As a default, we used five bins for the histogram, where the user can change the number of bins. Besides the distribution, each plot shows the density of an attribute combination using a yellow-to-blue color scale. For this, a counter for each plot pixel is increased when the corresponding combination occurs. Blueish regions indicate often occurring values, whereas yellow areas represent values that occur only at few regions. To ensure comparability between the two datasets, statistical plots showing the same combination between the upper and lower matrix, e.g, the top right entry and bottom left entry, are depicted within the same attribute range. The attribute range depends on the minimum and maximum values of the respective scalar fields of both datasets. During animation, the plots are updated to show the temporal development of the scalar distributions.
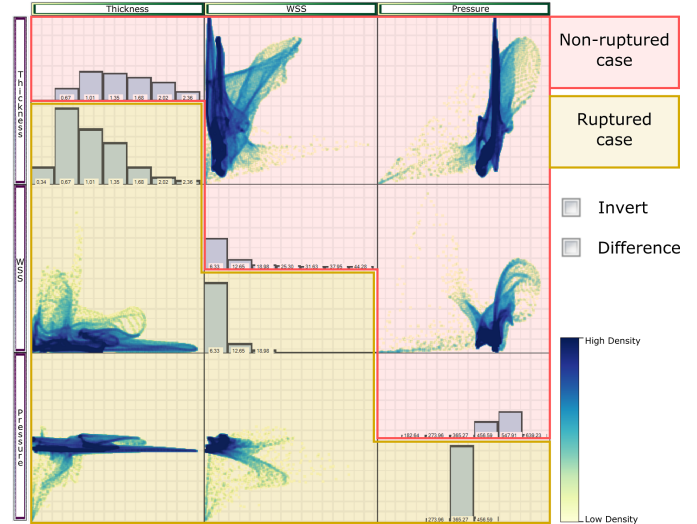

Fig. 8. Attribute analysis using statistical plots. For each combination, a density plot and histograms of the quantities are drawn, where the upper and lower triangular matrix represent different cases.

Comparative Scatterplots. Comparing two cases requires to mentally rotate the plots in the lower triangular matrix around 90°. To further facilitate such comparisons, the plots in the non-diagonal entries of the lower matrix can be transposed. Fig. 9 shows this for the combination of WSS and pressure for an aneurysm before (upper matrix) and after treatment (lower matrix). The first image represents the second entry of the first row in the matrix and the second image represents the bottom left matrix entry. Activating the transposed view flips the scatterplot orientation of the bottom left matrix entry, where the axis labels at the matrix sides stay the same. Then, the scatterplots before and after treatment have the same orientation, which facilitates their comparison. Moreover, a difference visualization can be activated showing changes between the cases using a gray-to-red color scale, see Fig. 9 (right). For this purpose, the lower matrix entries are used.

Fig. 9. Scatterplot-based comparison of WSS and pressure before and after stenting. The user has the possibility to invert the scatterplots of the lower triangular matrix and to activate a difference visualization that highlights changes after treatment.

High attribute values represented by red areas do not longer exist after stenting, since there is a positive difference. Only smaller attribute values represented by white-to-gray areas exist after stenting. With this, the expert can immediately see if attribute values could be reduced by using a specific stent configuration. Deactivating this rendering reloads the original scatterplots of the second case. In case that more stents were simulated, the user can select which scenario should be presented in the upper and lower matrix to compare the results.

5.4 Multi-Field Analysis on the Aneurysm Surface

The 3D and 2D aneurysm visualizations provide a detailed exploration of high-risk wall regions over the cardiac cycle. To create a spatial correlation between both views, the ostium area on the 3D mesh and the 2D map is highlighted in color. In case of post-treatment data, the 3D view shows also existing stent configurations. The 2D map gives a quick overview, whereby scalar quantities can be explored without occlusions (R. 2). In the following, we explain several techniques to analyze two scalar fields simultaneously on the 2D map as well as on the 3D surface to investigate possible rupture-prone correlations.

5.4.1 Simultaneous Exploration of Scalar Fields

Meuschke et al. [35] presented an approach to display two scalar fields simultaneously. The first attribute is color-coded and the second is visualized by an image-based hatching scheme, see Fig. 10 (left). The stronger the strokes, the higher the scalar value. However, the hatching discretizes the data range into four patterns, which restricts the quantitative analysis of the scalar field.

Color + Hatching   Checkerboard: $\gamma = -0.5$ Checkerboard: $\gamma = 0.0$ Checkerboard: $\gamma = 0.5$
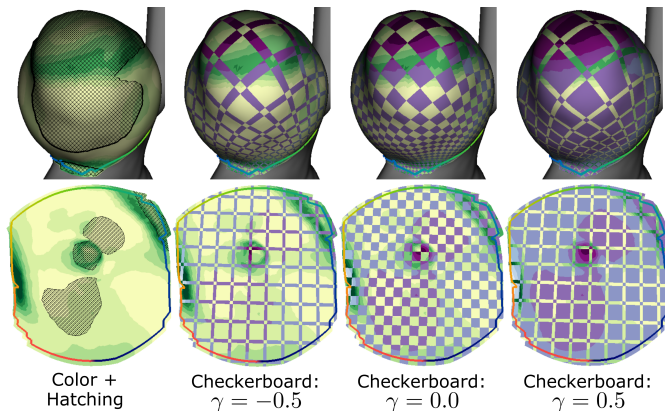
Fig. 10. Two visualization techniques showing two scalar fields on the 3D mesh and the 2D map. Left, WSS is represented by hatching and the wall deformation is color-coded. Right, a checkerboard visualization shows the WSS by a light purple-to-dark purple scale and the wall deformation by a yellow-to-green color scale. The corresponding γ-values are presented below.

To avoid this, we developed a checkerboard visualization that allows a simultaneous exploration of two attributes (R. 1) by generating a linear transition between them, see Fig. 10. For this, we divided the 2D map into a grid of size $num_x \times num_y$, where num_x, num_y yield the number of cells in x and y direction, respectively. As default, we set $num_x = num_y = 20$, but these values can be adjusted by the user. Additionally, we provide a slider ranging from $\gamma \in [-1, 1]$, emphasizing the first or the second field. Setting $\gamma = -1$ shows the first scalar field only, if we set $\gamma = 1$ only the second quantity is displayed. The continuous value γ provides a smooth transition from both states, where $\gamma = 0.0$ results in an equal distribution of both fields. The pseudo-code for the checkerboard depiction is provided as supplemental material.

5.4.2 Time-Dependent Attribute Visualization using Glyphs

As we deal with time-dependent data, the attributes on the aneurysm change during the cardiac cycle. For a fast overview of the data, we employ 3D violin surfaces to show the temporal behavior of up to two attributes (R. 5), which are inspired by the pencil glyphs [48].

Fig. 11. Glyphs to depict time-dependent attributes. The gray disc shows the current time step, where the lower end of the glyph represents t_0. Left, the glyph's color c and radius r represent the WSS. Right, WSS is color-coded and r visualizes pressure.

Basically, we create a cylinder with a fixed number of points for the radius and for the height, see Fig. 11. The first attribute is depicted using a yellow-to-green color scale. For visualizing the second attribute, every point of the cylinder is shifted along the normal such that the radius corresponds to the specific scalar value. The current time is indicated by a disc at the corresponding glyph height. Fig. 11 (left) shows an example, where the WSS is encoded by color and radius, where the right glyph encodes WSS by color and pressure by the radius.
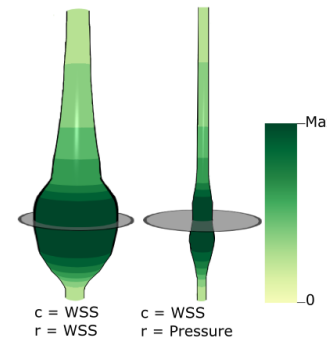
The glyphs are placed on the 2D map at regular grid points. For the sampling rate, we use 10 % of the map's extent in x and y direction. Additionally, the user can add glyphs at certain regions by clicking on the map. This allows to analyze quantities at different points during the cardiac cycle.

5.5 Attribute-Based Clustering

To more easily detect regions of interesting attribute combinations, we provide a clustering scheme that results in surface regions with similar scalar values. In contrast to Glaßer et al. [17], who defined a fixed combination of WSS and wall thickness for a single time step, different combinations over time are possible. In our tool, we list the given n attributes, noted here with $s_1, s_2, \ldots, s_n$. To support the process of

6

combining attributes for clustering, we assist the experts with different facilities. First, the expert can set individual weights $w_1, w_2, \ldots, w_n$ for each attribute. Initially, we use $w_i = \frac{1}{n}$. Based on the selected weights, an overall scalar vector S is determined for every vertex i:

$$S_i = \left(\sqrt{w_1} s_1(i) \quad \sqrt{w_2} s_2(i) \quad \ldots \quad \sqrt{w_n} s_n(i) \right)^T. \tag{1}$$

Furthermore, attributes can be normalized to the range $[0, 1]$, which is activated as default value. Moreover, some quantities might be more interesting if low values occur instead of high values, e.g., wall thickness. The expert may rather be interested in a cluster that exhibits high WSS and low wall thickness, cf. [17]. For this purpose, an attribute s_i can be inverted, where s_i is changed to $s_i' = (\max_x s_i(x)) - s_i$.

To identify surface regions with similar scalar values during the cardiac cycle, we incorporate the temporal component of attributes into the clustering. Based on the surface mesh, composed of vertices, we use a graph structure with edge costs. We follow an approach that resembles region growing-based segmentation where a seed point is used to initiate a growing process. While in image segmentation one structure is segmented by accumulating neighboring pixels that fulfill a condition, we apply this method to different parts of the data, effectively partitioning it like a clustering. As input, a weighted adjacency matrix is used. Besides region growing, more advanced clustering techniques such as hierarchical methods [16] or spectral clustering [45] could be used. However, these approaches need a full matrix, containing the pairwise similarity values for all vertices. On average, the aneurysm surface part in our cases consists of 5000 vertices and up to 93 simulated time steps. The resulting similarity matrix would have be a size of $n \cdot T \times n \cdot T$, with n the number of vertices and T the number of time steps. This would take more than 800 Gigabytes of memory. Using the region growing, a sparse matrix can be calculated, comprising 11-13 Megabytes. First, we explain how to apply the clustering on the surface within a fixed point in time t. The adjacency matrix A is constructed by: $A_{ij} = 1$, if $(i, j) \in E$ and 0 otherwise, where E denotes the edges. Using A and a start point, region growing is applied. For start point selection, we sort the vertices according to $\|S_i(t)\|$, where S_i is the overall scalar vector, cf. Equation 1. The vertex i with the lowest $\|S_i\|$ is used as start point. Then, all vertices j that are adjacent to i are determined using A. If $(\|S_i(t) - S_j(t)\|) < \theta$ holds, the vertex j is incorporated into the current cluster, where θ is a predefined threshold. This is repeated until no more adjacent point exists that fulfills θ. Then, the next point from the sorted list that was not yet visited is used as new start point. For θ, we use the average of $\|S_i(t) - S_j(t)\|$ for all point pairs on the surface. Significantly higher values result in very small clusters, where much lower values result in quite large clusters with a broad distribution of scalar values within a cluster. However, the user can adjust θ.

To extend the method to time-varying data, we construct a temporal adjacency matrix W. The matrix W is of size $n \cdot T \times n \cdot T$. Then, W has repetitive matrices A along the diagonal blocks (T times) and the identity matrix on the off-diagonal blocks. By constructing W, for a fix point in time it is simply the adjacency matrix, but changing the time from t_i to t_{i+1} only identical vertices are connected for the underlying graph, see Fig. 12. With this, the sparse matrix can be generated. Then, if $(\|S_i(t_k) - S_i(t_{k+1})\|) < \theta$ holds, the vertex i at time t_{k+1} is incorporated into the current cluster. The clustering yields non-overlapping regions, where each surface point is assigned to a cluster. It takes between 3.5 and 15 s, depending on the amount of vertices and time steps. Fig. 13 shows exemplary results for three time steps t_1, t_2, and t_3, where the Mises stress and WSS is clustered using $w_1 = w_2 = 0.5$. To assess the homogeneity of regions (R. 4), for each cluster c_i a risk factor $R_i = \frac{1}{\#c_i} \sum_{j \in c_i} \|S_j\|$ is determined, where $\#c_i$ is the size of the cluster. Then, R_i is color-coded using a light yellow-to-red color scale. Inhomogeneous regions show a larger number of clusters with strongly varying risk values, whereas homogeneous regions exhibit less clusters with similar risk values. For clustering, we averaged the edge weights of every cluster and used this value to color-code the cluster results. Note that we also weighted the edge weights with their length, but we could not see any difference.
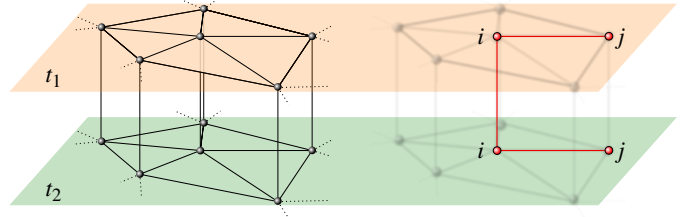

Fig. 12. For a start vertex i at time t_1 the matrix W is used for region growing. Here, $(\|S_i(t_1) - S_j(t_1)\|) < \theta$, $(\|S_i(t_1) - S_i(t_2)\|) < \theta$, and $(\|S_i(t_1) - S_j(t_2)\|) < \theta$ hold, thus, these vertices are included into the cluster of vertex i at time t_1.
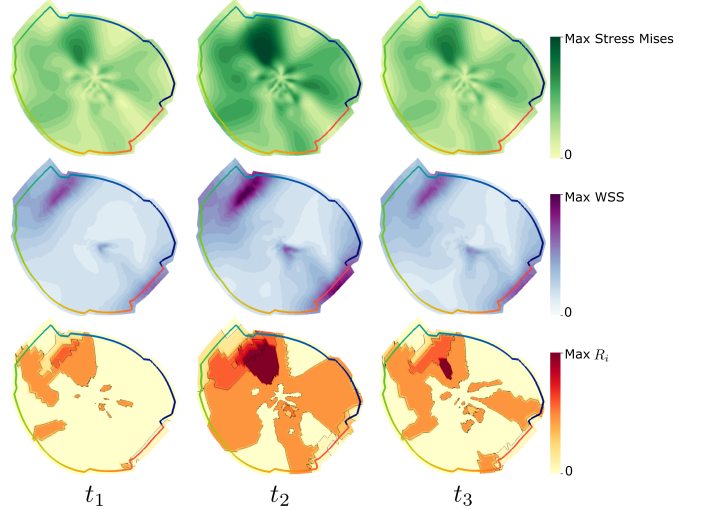

Fig. 13. Clustering results for three time steps t_1, t_2, and t_3. Here, the Mises stress (top) and WSS (middle) is clustered with $w_1 = w_2 = 0.5$. The resultant risk factor R_i is color-coded for each cluster (bottom). The black contours show the cluster borders.

5.6 Brushing and Linking

The analysis of scalar quantities requires brushing and linking facilities that allow the user to explore the aneurysm morphology at interesting regions. In case the scatterplot shows interesting combinations, the expert may analyze the morphological attributes in 3D or on the 2D map. Therefore, the user can brush regions in the scatterplot, which are immediately highlighted on the 3D surface and 2D map (R. 6), see Fig. 14. The user can also mark regions on the 3D surface or the 2D map and the corresponding regions in the other views are highlighted. For a more quantitative evaluation, statistical diagrams can be activated, see Fig. 14. A diagram is rendered for each attribute and shows the minimum, maximum as well as mean value of the brushed points over time. Moreover, the areas of the 25 % and 75 % quantile are highlighted. For scalar values, the overall mean value per attribute and variance is shown. This quantitative region analysis can also either be activated for a user-selected cluster, where the clustered attributes are depicted, or a selected region in 2D or 3D based on the discretized color scale.

Besides brushing, the 2D map and the 3D surface are linked to each other. Selecting a specific point on the 2D map automatically changes the camera perspective to the corresponding 3D position in a smooth way. In 3D, a green sphere appears at this position. Thus, interesting regions can be explored in 3D without a manual search.

6 EVALUATION

The evaluation comprises three parts, where eight domain experts participated forming three expert groups (EG). EG1 comprises four doctors P1 to P4 (10, 13, 18, 25 years experience in radiology). Two CFD engineers, P5 and P6, who deal with the hemodynamic analysis of cerebral aneurysms (4 and 7 years of experience) form EG2. EG3
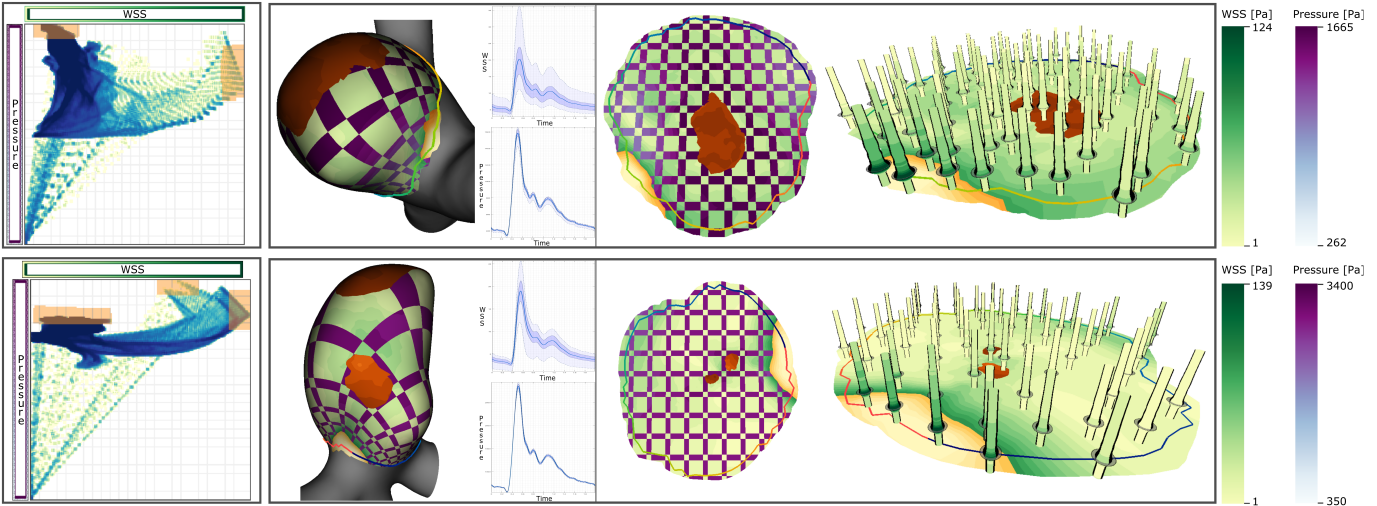
Fig. 14. Two aneurysms with a size of $2.8\,mm$ (top) and $5.3\,mm$ (bottom) that were assessed as less rupture-prone based on morphological features. The first aneurysm shows suspicious regions with an increased WSS. The second aneurysm ruptured at the dome, where a high pressure occurs.

consists of two experts for medical visualizations P7, P8 (4 and 6 years of experience). P4 and P6 also supported us with defining the requirements, see Sec. 4. First, we presented the interaction possibilities and explained definable user values, e.g., the slider and number of grids using an exemplarily dataset. Based on this, a case study was carried out with EG1 for different cases, see Sec. 6.1. Then, we asked all EG's to fill out a questionnaire to assess the suitability of our visualizations, see Sec. 6.2. For this, different exemplarily datasets are presented to EG2 and EG3, since they did not participated in the case study. Moreover, EG2 was asked to focus on whether the distribution of attributes in terms of physical plausibility can be perceived, as this was described as an important task of CFD experts, see Sec. 4. Finally, we compared our visualizations to related methods also dealing with the simultaneous exploration of multiple attributes, see Sec. 6.3.

6.1 Case Study

Our main goal is to improve rupture risk assessment and treatment decision. To evaluate if our tool fulfills this, a case study was performed focused on saccular aneurysms, see Tab. 1. Fusiform aneurysms are usually treated surgically due to occurring symptoms. So, in the past the assessment of blood flow data played a minor role. More recently, medical studies investigated endovascular treatment options for fusiform aneurysms [32, 38]. These treatments could be an alternative to surgical interventions. However, also more complications occurred, as the current stent design seems not to be optimal for fusiform aneurysms. Thus, improving treatment is an active research area. Since, we have no treated data of these aneurysms, we asked for the usefulness to be able to handle fusiform aneurysms. The experts appreciated this, since in the near future simulated data for treatment assessment will be available, where the 2D map would simplify data analysis.

First, we asked EG1 to assess the rupture risk and treatment necessity based on morphological features for C4-C16. Note that they were not aware of the condition (ruptured or not). Among non-ruptured cases were two smaller (diameter $\leq 7\,mm$), morphologically inconspicuous aneurysms (C4, C5) for which a low risk was estimated, see Fig. 14 (top row). For C6, the doctors were unsure. Only considering the diameter ($8\,mm$), they advised to treat, but no blebs were existing, so the aneurysm could also be observed first. The remaining five cases are considerably larger (about $10\,mm$), where three of them have additional blebs, so the doctors estimated an increased risk and advised to treat them. They predicted an increased risk for the ruptured cases C9, C10 and C16 due to blebs. For two cases, they were again uncertain, as C11 has a similar size and less risky appearing morphology to C6. C12 is even smaller ($5.3\,mm$), see Fig. 14 (bottom row), but its morphology seems a bit more conspicuous than, e.g., C5. But the doctors stated that such cases could also be observed for a while.

Afterwards, our tool was used for exploration, where we observed two workflows, one for risk analysis and one for treatment assessment. Risk analysis was explained as highly important for low-risk appearing aneurysms, having a small size or at least no blebs such as C4-C6 or C11-C12. The goal is to find high-risk attribute correlations on the more harmless appearing surface. For this purpose, the circle plot was used first to identify time steps that show interesting characteristics. It was stated that the circle plot is also appropriate to decide which attributes would be meaningful for the provided clustering. Then, the scatterplots and histograms are used to explore the scalar distributions, since colored regions in the circle plot could represent singular outliers. Moreover, they brushed regions on the map, where the glyphs show increased WSS and pressure values. Afterwards, they activated the statistical diagrams to analyze the brushed regions more quantitatively. Also, the checkerboards are used to analyze attributes. We observed that the experts set $\gamma = 0$ and set the number of cells $num_x = num_y = 25$. Here, the spoken comment of P4 was that he first searches for abnormalities of two quantities. Then, setting $\gamma = 1$ and $\gamma = -1$ helps to get an impression of the regional behavior of the attribute. With this, increased pressure values are detected on the dome region, which was the rupture site of C12, see Fig. 14 (bottom row). So a risk analysis based on morphological criteria was not appropriate. However, C5 has similar WSS at the ostium region, which could also be a rupture-prone area. Similar areas where found for C6 and C11, so the experts get more certain that these cases are more risky, where they were able to detect the rupture site of C11. For C4 no similar risky regions were found, so the experts maintained their opinion of a smaller risk.

For risky appearing aneurysms, the treatment workflow follows. Here, we observed a more focused analysis of regions, where the experts already assume a higher risk. These regions are brushed on the surface and then the circle plot was used to analyze correlations. They selected regions within the plot and then the matrix view is used to investigate attribute distributions before and after treatment. They assessed how the scalar distributions are changing depending on the selected stent. If there is no clear changing of, e.g., the pressure values, the selected stent type or its location is probably not appropriate to prevent aneurysm inflow. For C16, four different stent configurations were simulated, where the experts decide for the fourth scenario to be the best, which is explained in more detail in Sec. 6.3.

6.2 Expert Feedback based on Questionnaire

After the case study, the experts filled out a questionnaire about the visualizations and their medical relevance using a five-point Likert scale ($--,-,\circ,+,++$). Meanwhile, we noted their spoken comments, which are summarized in the following. For further details, we provide the questionnaire and a detailed list of answers as supplemental material.

All experts emphasized the importance of analyzing different attributes to assess the aneurysm's state. They confirmed that the circle plot provides a fast overview of interesting time steps and attribute correlation. The suitability of the checkerboard to analyze two attributes simultaneously was rated more controversially. P2 and P4 argued that the hatching scheme more directly indicates possible attribute correlations, whereas the experts needed more time to get used to the checkerboard. However, they mentioned that the checkerboard allows a more quantitative comparison, which is less possible with the hatching. The 3D glyphs were perceived as appropriate to depict the temporal behavior of two attributes. In addition, the brushing was described as helpful to establish a spatial correlation between the views and to identify rupture-prone regions. The scatterplots showing attributes before and after treatment or between ruptured and non-ruptured datasets help to assess treatment success and rupture risk. Finally, the clustering and color-coding of the risk factor was rated as a great improvement, where homogeneous and inhomogeneous regions can be detected.

6.3 Comparison with Related Approaches

First, we compared our cylinder glyphs to the bar charts by Meuschke et al. [35] that also show two time-dependent attributes, see Sec. 2.2. Then, we compared our circular plot to the pencil glyphs by Tominski et al. [48], which are designed to show multiple attributes over time. Finally, we compared our tool to the system of van Pelt et al. [51], where flower-shaped glyphs are used to compare the influence of multiple stent configurations. Informal expert interviews are carried out to investigate, if our methods are more suitable to analyze multiple attributes.

We presented different settings of two attributes to all EG's. They preferred our cylinder glyphs, because the bar charts do not allow to perceive the temporal behavior of the attributes at a glance. Instead, the animation must always be viewed over the entire cycle to find hotspots. Moreover, it is difficult to locate the corresponding anatomical position on the aneurysm, since the bar charts are displayed over a 2D aneurysm map. Our glyphs can be easy located, since they are directly placed on the map. Furthermore, the experts preferred our circular plot compared to the pencil glyphs [48]. The main criticism of the pencil glyphs was that a lot of manual rotation was required to explore attributes. It is difficult to find an appropriate camera perspective for more than three attributes, which complicates the exploration of correlations.

The system comparison was performed for C16, which was also used by van Pelt et al. [51]. It was virtually stented with four stent configurations. Since, our tool is focused on the analysis of scalar attributes on the wall, we disabled the exploration of internal flow structures in the other system. In their evaluation, two CFD experts were asked to identify the stent leading to lowest WSS at interesting locations such as the ostium and the additional bleb. We also asked our experts to perform this task, where we noted their spoken comments. For this purpose, we split them into two groups, comprising two clinicians as well as one CFD and one visualization expert, respectively. The first group started with the tool by van Pelt et al. [51] and proceed with our tool. For the second group, this was performed vice versa.

The feedback of both groups was quite similar. All experts criticized the high rotation and zooming effort necessary for the flower glyphs to detect critical regions. Comparing stents at different surface locations is quite challenging, since the varying radii of the disks only provide indirectly quantitative information. In addition, the clinicians and CFD experts criticized the restriction to five presented time steps as well as that only one attribute can be explored. With this, hot spots of fluid-wall interaction can be missed. Due to these limitations, the experts were unsure about the optimal stent, since configuration 1 and 4 seems to lead to similar WSS distributions. Using our tool, the experts described the decision-making process as much easier, as methods are provided to efficiently explore interesting regions. The experts brushed the ostium and bleb region and analyzed the corresponding areas within the comparative scatterplots for different stents. Due to the more quantitative data representation, the experts were able to observe that configuration 4 more strongly reduces WSS than configuration 1, which was also described as the best option by van Pelt et al. We provide some resulting images of this system comparison as supplemental material.

7 Discussion

The evaluation indicates that our tool improves risk assessment and decision-making. The combination of the circle plot together with statistical plots as well as 2D and 3D views allows an efficient exploration of attributes. The physicians were able to perform a more in-depth analysis leading to different or more certain assessments of rupture risk and treatment options. Moreover, our methods outperform other techniques [35, 48, 51] to explore scalar data. Since the checkerboard was discussed more controversially, physicians could imagine to use two juxtaposed maps, where each shows one attribute, as doctors are used to mentally combine two views. However, the other experts described the detection of scalar correlations as difficult using two maps.

Limitations. According to the matrix view, the display size determines the number of attributes that can be visualized. We used a display with a resolution of 2560×1440 pixels. With this, up to five attributes can be depicted so that all four views exhibit an appropriate size. Similar to this is the number of displayed attributes within a cell of the circular plot. By default, a maximum of six regions are distinguished, which can be well perceived. Theoretically, the user can brush more than six regions on the surface, which are displayed within the plot. Then, reading becomes probably more difficult. However, in most cases experts are only interested in a few interesting regions, such as blebs.

Improvements. The experts asked for visual hints that encode distortions between the 2D map and the 3D depiction, i.e., showing a grid in both views. For placing glyphs, the experts suggested an importance-driven sampling such that glyphs appear where minimum and maximum values occur. Moreover, P8 suggested filtering glyphs by attribute ranges, which would help to focus on high-risk regions. It may also be helpful to explore aneurysm data after other treatment options, such as coiling. This would require a visualization of the used coils. According to the clustering, one expert asked for an overview that shows the progress of the cluster over time. This would allow to explore the extent to which clusters change over time. Moreover, two experts asked for a stronger user integration by providing interesting attribute ranges.

8 Conclusion and Future Work

We presented a tool to explore aneurysms regarding the rupture risk and treatment planing. For this, we came up with a list of requirements that should be fulfilled. Regarding our evaluation, our tool was considered successful w.r.t. the requirements. Decision-making is supported by linked views to analyze attribute correlations over the cardiac cycle.

At the moment there is no essential knowledge to reliably calculate a rupture probability. It is assumed that rupture is caused by the combination of different attributes, although little is known about the exact influence of individual quantities. Through the targeted exploration of suspicious surface areas, our tool supports experts to better understand the causes of rupture. This is especially important for smaller aneurysms, which seem to be morphologically less dangerous. Therefore, our tool supports experts in finding a general risk factor. Besides the time-dependent analysis of attributes, our tool allows to compare the results of treatment options. For this, also stated by our domain experts, our tool supports physicians in their decision-making process.

For future work, the physicians proposed a workflow using the clustering for a larger aneurysm study. They want to explore attribute combinations at known rupture sites. Our clustering can be used to investigate the currently poorly understood influence of attributes on rupture by systematically changing their weights. If the cluster remain constant, the changed attribute has probably a lesser influence. The next steps are to brush regions of rupture and to analyze the data distribution. Moreover, we want to extend the mapping to the parent vessel geometry. This would enable an analysis of the effects of different stents on the blood flow within adjacent vessels. Furthermore, we want to provide a visual exploration of qualitative flow patterns that can be related to rupture or treatment success.

REFERENCES

[1] P. Angelelli and H. Hauser. Straightening tubular flow for side-by-side visualization. *IEEE Trans Vis Comput Graph*, 17(12):2063–70, 2011.

[2] O. K.-C. Au, C.-L. Tai, H.-K. Chu, D. Cohen-Or, and T.-Y. Lee. Skeleton extraction by mesh contraction. *ACM Trans Graph*, 27(3):1–10, 2008.

[3] P. Berg, L. Daróczy, and G. Janiga. Virtual stenting for intracranial aneurysms: A risk-free, patient-specific treatment planning support for neuroradiologists and neurosurgeons. In *Computing and Visualization for Intravascular Imaging and Computer-Assisted Stenting*, pp. 371–411. 2017.

[4] P. Berg, C. Roloff, O. Beuing, S. Voss, and et al. The Computational Fluid Dynamics Rupture Challenge 2013–Phase II: Variability of Hemodynamic Simulations in Two Intracranial Aneurysms. *J Biomech Eng*, 137(12):121008, 2015.

[5] P. Berg, D. Stucht, G. Janiga, O. Beuing, O. Speck, and D. Thévenin. Cerebral blood flow in a healthy circle of willis and two intracranial aneurysms: computational fluid dynamics versus four-dimensional phase-contrast magnetic resonance imaging. *Biomed Eng*, 136(4):041003, 2014.

[6] R. Blankena, R. Kleinloog, B. Verweij, P. van Ooij, B. Ten Haken, Luijten, and et al. Thinner regions of intracranial aneurysm wall correlate with regions of higher wall shear stress: A 7T MRI study. *Am J Neuroradiol*, 2016.

[7] R. Borgo, J. Kehrer, D. H. Chung, E. Maguire, and et al. Glyph-based visualization: Foundations, design guidelines, techniques and applications. *Eurographics*, pp. 39–63, 2013.

[8] J. R. Cebral, F. Mut, J. Weir, and C. M. Putman. Association of hemodynamic characteristics and cerebral aneurysm rupture. *Am J Neuroradiol*, 32(2):264–70, 2011.

[9] J. R. Cebral, M. Vazquez, D. M. Sforza, G. Houzeaux, and et al. Analysis of hemodynamics and wall mechanics at sites of cerebral aneurysm rupture. *J Neurointerv Surg*, 7(7):530–36, 2015.

[10] M. D. Cerqueira, N. J. Weissman, V. Dilsizian, A. K. Jacobs, and et al. Standardized myocardial segmentation and nomenclature for tomographic imaging of the heart: a statement for healthcare professionals from the cardiac imaging committee of the council on clinical cardiology of the american heart association. *J Am Soc Echocardiogr*, 15(5):463–67, 2002.

[11] K. Crane, C. Weischedel, and M. Wardetzky. Geodesics in Heat: A New Approach to Computing Distance Based on Heat Flow. *ACM Trans Graph*, 32:152, 2013.

[12] C. Díaz and L. A. Robles. Fast noncontinuous path phase-unwrapping algorithm based on gradients and mask. In *Iberoamerican Congress on Pattern Recognition*, pp. 116–23, 2004.

[13] H. Doleisch, M. Gasser, and H. Hauser. Interactive feature specification for focus+context visualization of complex simulation data. In *Proc. of IEEE/EG VisSym*, pp. 239–48, 2003.

[14] H. Doleisch, M. Mayer, M. Gasser, R. Wanker, and H. Hauser. Case study: Visual analysis of complex, time-dependent simulation results of a diesel exhaust system. In *Proc. of IEEE/EG VisSym*, pp. 91–6, 2004.

[15] P. Dyverfeldt, M. Bissell, A. J. Barker, A. F. Bolger, and et al. 4D Flow Cardiovascular Magnetic Resonance Consensus Statement. *J Cardiovasc Magn Reson*, 17(1):72, 2015.

[16] L. Ferreira and D. B. Hitchcock. A comparison of hierarchical methods for clustering functional data. *Commun Stat Simul Comput*, 38(9):1925–49, 2009.

[17] S. Glaßer, K. Lawonn, T. Hoffmann, M. Skalej, and B. Preim. Combined visualization of wall thickness and wall shear stress for the evaluation of aneurysms. *IEEE Trans Vis Comput Graph*, 20(12):2506–15, 2014.

[18] L. Goubergrits, J. Schaller, U. Kertzscher, N. van den Bruck, K. Poethkow, C. Petz, and et al. Statistical wall shear stress maps of ruptured and unruptured middle cerebral artery aneurysms. *J R Soc Interface*, 9(69):677–88, 2012.

[19] D. L. Gresh, B. E. Rogowitz, R. L. Winslow, D. F. Scollan, and C. K. Yung. WEAVE: a system for visually linking 3D and statistical visualizations applied to cardiac simulation and measurement data. In *Proc. of IEEE Visualization*, pp. 489–92, 2000.

[20] K. C. Gurijala, R. Shi, W. Zeng, X. Gu, and A. Kaufman. Colon flattening using heat diffusion riemannian metric. *IEEE Transactions on Visualization and Computer Graphics*, 19(12):2848–57, 2013.

[21] S. Haker, S. Angenent, A. Tannenbaurn, and R. Kikinis. Nondistorting flattening maps and the 3-d visualization of colon ct images. *IEEE Transactions on Medical Imaging*, 19(7):665–70, 2000.

[22] G. Janiga, L. Daróczy, P. Berg, D. Thévenin, M. Skalej, and O. Beuing.

[23] Automatic CFD-based optimization of a flow diverter treatment for a patient-specific giant aneurysm. *J Biomech*, 48(14):3846–52, 2015.

[23] J. Kehrer, P. Muigg, H. Doleisch, and H. Hauser. Interactive visual analysis of heterogeneous scientific data across an interface. *IEEE Trans Vis Comput Graph*, 17(7):934–46, 2011.

[24] J. Kiefer. Sequential minimax search for a maximum. *Proc. of the American Mathematical Society*, 4:502–6, 1953.

[25] G. Kindlmann. Superquadric tensor glyphs. In *Proc. of Joint Eurographics - IEEE Visualization*, pp. 147–54, 2004.

[26] B. Köhler, M. Meuschke, U. Preim, K. Fischbach, M. Gutberlet, and B. Preim. Two-Dimensional Plot Visualization of Aortic Vortex Flow in Cardiac 4D PC-MRI Data. In *Proc. of Bildverarbeitung für die Medizin*, pp. 257–61, 2015.

[27] J. Kreiser, M. Meuschke, G. Mistelbauer, B. Preim, and T. Ropinski. A Survey of Flattening-Based Medical Visualization Techniques. *Computer Graphics Forum*, 2018.

[28] R. Lall, C. Eddleman, B. Bendok, and H. Batjer. Unruptured intracranial aneurysms and the assessment of rupture risk based on anatomical and morphological factors: Sifting through the sands of data. *Neurosurg Focus*, 26(5):E2, 2009.

[29] J.-W. Lankhaar, M. Hofman, J. T. Marcus, J. J. Zwanenburg, T. J. Faes, and A. Vonk-Noordegraaf. Correction of phase offset errors in main pulmonary artery flow quantification. *Journal of Magnetic Resonance Imaging*, 22(1):73–79, 2005.

[30] K. Lawonn, R. Gasteiger, and B. Preim. Adaptive surface visualization of vessels with animated blood flow. *Comp Graph Forum*, 33(8):16–27, 2014.

[31] B. Lévy, S. Petitjean, N. Ray, and J. Maillot. Least squares conformal maps for automatic texture atlas generation. *ACM Trans Graph*, 21(3):362–71, 2002.

[32] P. B. Metzger, E. R. Novero, F. H. Rossi, S. M. Moreira, H. A. Barbato, N. M. Izukawa, V. L. A. d. Marco, M. N. Cano, and A. M. Kambara. Endovascular treatment of abdominal aortic aneurysms with complex anatomy: preliminary results of the second generation stent graft with a dual-ring design. *Revista Brasileira de Cardiologia Invasiva*, 20(1):69–76, 2012.

[33] M. Meuschke, T. Günther, R. Wickenhöfer, M. Gross, B. Preim, and K. Lawonn. Management of Cerebral Aneurysm Descriptors based on an Automatic Ostium Extraction. *IEEE Comput Graph Appl*, 38(3):58–72, 2018.

[34] M. Meuschke, B. Köhler, U. Preim, B. Preim, and K. Lawonn. Semi-automatic Vortex Flow Classification in 4D PC-MRI Data of the Aorta. *Comp Graph Forum*, 35(3):351–60, 2016.

[35] M. Meuschke, S. Voß, O. Beuing, B. Preim, and K. Lawonn. Combined visualization of vessel deformation and hemodynamics in cerebral aneurysms. *IEEE Trans Vis Comput Graph*, 23(1):761–70, 2017.

[36] M. Meuschke, S. Voß, O. Beuing, B. Preim, and K. Lawonn. Glyph-based comparative stress tensor visualization in cerebral aneurysms. *Comp Graph Forum*, 36(3):99–108, 2017.

[37] T. Mönch, M. Neugebauer, and B. Preim. Optimization of vascular surface models for computational fluid dynamics and rapid prototyping. In *Workshop on Digital Engineering*, pp. 16–23, 2011.

[38] S. J. Monteith, A. Tsimpas, A. S. Dumont, S. Tjoumakaris, L. F. Gonzalez, R. H. Rosenwasser, and P. Jabbour. Endovascular treatment of fusiform cerebral aneurysms with the pipeline embolization device. *J Neurosurg*, 120(4):945–54, 2014.

[39] P. Mullen, Y. Tong, P. Alliez, and M. Desbrun. Spectral conformal parameterization. In *Proc. of Symp Geom Process*, pp. 1487–94, 2008.

[40] M. Neugebauer, R. Gasteiger, O. Beuing, V. Diehl, M. Skalej, and B. Preim. Map displays for the analysis of scalar data on cerebral aneurysm surfaces. In *Comput Graph Forum*, vol. 28 (3), pp. 895–902, 2009.

[41] L. Phan, K. Courchaine, A. Azarbal, D. Vorp, C. Grimm, and S. Rugonyi. A Geodesics-Based Surface Parameterization to Assess Aneurysm Progression. *J Biomech Eng*, 138(5):054503, 2016.

[42] A. Rocha, U. Alim, J. Silva, and M. Sousa. Decal-maps: Real-time layering of decals on surfaces for multivariate visualization. *IEEE Trans Vis Comput Graph*, 23(1):821–30, 2017.

[43] T. Ropinski, S. Oeltze, and B. Preim. Survey of glyph-based visualization techniques for spatial multivariate medical data. *Computers & Graphics*, 35(2):392–401, 2011.

[44] J. Schöberl. An advancing front 2D/3D- mesh generator based on abstract rules. *Comput Vis Sci*, 1:41–52, 1997.

[45] J. Shi and J. Malik. Normalized cuts and image segmentation. *IEEE Trans*

Pattern Anal Mach Intell, 22(8):888–905, 2000.

[46] H. Steinmetz. Unrupturierte intrakranielle aneurysmen. *Der Nervenarzt*, 82(10):1343–50, 2011.

[47] J. Tao, X. Huang, F. Qiu, C. Wang, J. Jiang, C.-K. Shene, Y. Zhao, and D. Yu. VesselMap: A web interface to explore multivariate vascular data. *Computers & Graphics*, 59:79–92, 2016.

[48] C. Tominski, P. Schulze-Wollgast, and H. Schumann. 3D information visualization for time dependent data on maps. In *Proc. of IEEE Information Visualisation*, pp. 175–81, 2005.

[49] A. Valencia, D. Ledermann, R. Rivera, E. Bravo, and et al. Blood flow dynamics and fluid-structure interaction in patient-specific bifurcating cerebral aneurysms. *Int J Numer Meth FL*, 58(10):1081–1100, 2008.

[50] R. Van Pelt, J. Bescos, M. Breeuwer, R. Clough, E. Groller, B. ter Haar Romenij, and A. Vilanova. Exploration of 4d mri blood flow using stylistic visualization. *IEEE Trans Vis Comput Graph*, 16(6):1339–47, 2010.

[51] R. van Pelt, R. Gasteiger, K. Lawonn, M. Meuschke, and B. Preim. Comparative blood flow visualization for cerebral aneurysm treatment assessment. *Comput Graph Forum*, 33(3):131–40, 2014.

[52] M. J. Wermer, I. C. van der Schaaf, A. Algra, and G. J. Rinkel. Risk of rupture of unruptured intracranial aneurysms in relation to patient and aneurysm characteristics. *Stroke*, 38(4):1404–10, 2007.

[53] R. Zayer, C. Rössl, and H.-P. Seidel. Discrete tensorial quasi-harmonic maps. In *Proc. of IEEE Shape Modeling and Applications*, pp. 276–85, 2005.